Supporting Information

Pseudocapacitive trimetallic NiCoMn-111 perovskite fluorides for advanced Li-ion supercabatteries

Tong Yan[1], Yongfa Huang[1], Rui Ding[*], Wei Shi, Danfeng Ying, Ziyang Jia, Caini Tan, Yuxi Huang, Xiujuan Sun, and Enhui Liu

Key Laboratory of Environmentally Friendly Chemistry and Applications of Ministry of Education, College of Chemistry, Xiangtan University, Hunan 411105, P.R. China

[*]**Corresponding Author**

Emails: drm8122@163.com; drm8122@xtu.edu.cn (Rui Ding)

[1]The authors contribute equally to the work.

Table of Contents

LICs: 4.0 V (a, e), 4.3 V (b, f),4.5 V (c, g) and 4.7 V (d, h).

Fig. S17 Performance of AC, AC+LMO and AC+LFP cathode: CV plots at 0.5-80 mV s^{-1} (a, d, g), GCD curves at 1 A g^{-1} (b, e, h) and GCD curves at 0.1-3.2 A g^{-1} (c, f, i).

Fig. S18 The CV plots at 10-160 mV s^{-1} and GCD curves at 0.5-16 A $g^{-1}$of $8^{\#}$-P//AC+LFP(1:1) LIC/LIB hybrids: 4.0 V (a, e), 4.3 V (b, f),4.5 V (c, g) and 4.7 V (d, h).

Table S1 Chemicals, reagents and materials used in the study.

Table S2 The synthesis conditions of nine KNCMF-111 samples.

Table S3 Specific capacity (mAh g^{-1}) and cycling behavior of $1^{\#}$-$9^{\#}$, AC, AC+LMO (1:1) and AC+LFP (1:1) electrodes in non-aqueous system

Table S4 The design of electrode mass ratios of LICs and LICBs

Table S5 Specific capacity and cycling retention of KNCMF-111($8^{\#}$-P)//AC LICs under different working voltages

Table S6 Specific capacity and cycling retention of KNCMF-111($8^{\#}$-P)//AC+LFP LICBs under different working voltages

Table S7 A comparison for the performance of the KNCMF-111($8^{\#}$-P)//AC+LFP LICBs in the study with some reported LICs.

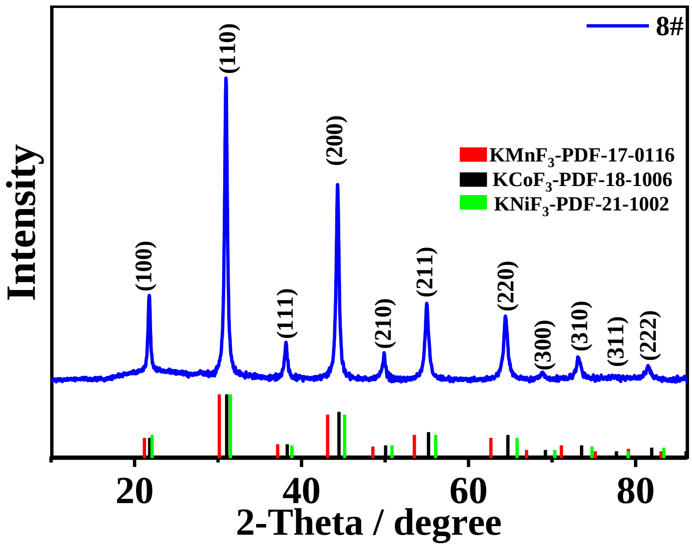

Fig. S1 The XRD pattern of $8^{\#}$ sample.

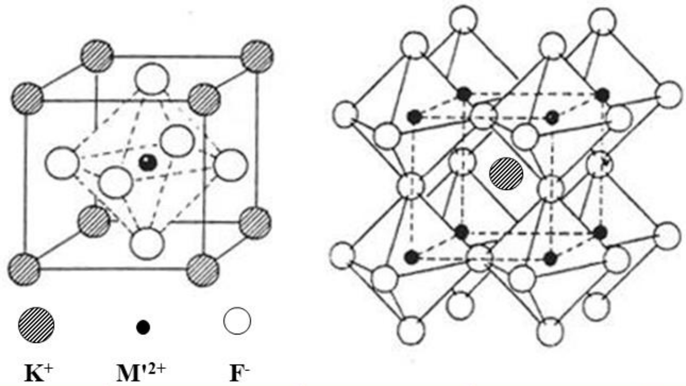

Sample	ICCD-PDF	Crystal system	Space group	Cell (a×b×c)/Å³
$KNiF_3$	21-1002	Cubic	Pm-3m	4.0127×4.0127×4.0127
$KCoF_3$	18-1006	Cubic	Pm-3m	4.0708×4.0708×4.0708
$KMnF_3$	17-0116	Cubic	Pm-3m	4.189×4.189×4.189

Fig. S2 The crystalline structures of perovskite $KM'F_3$ and crystalline parameters for $KNiF_3$, $KCoF_3$ and $KMnF_3$.

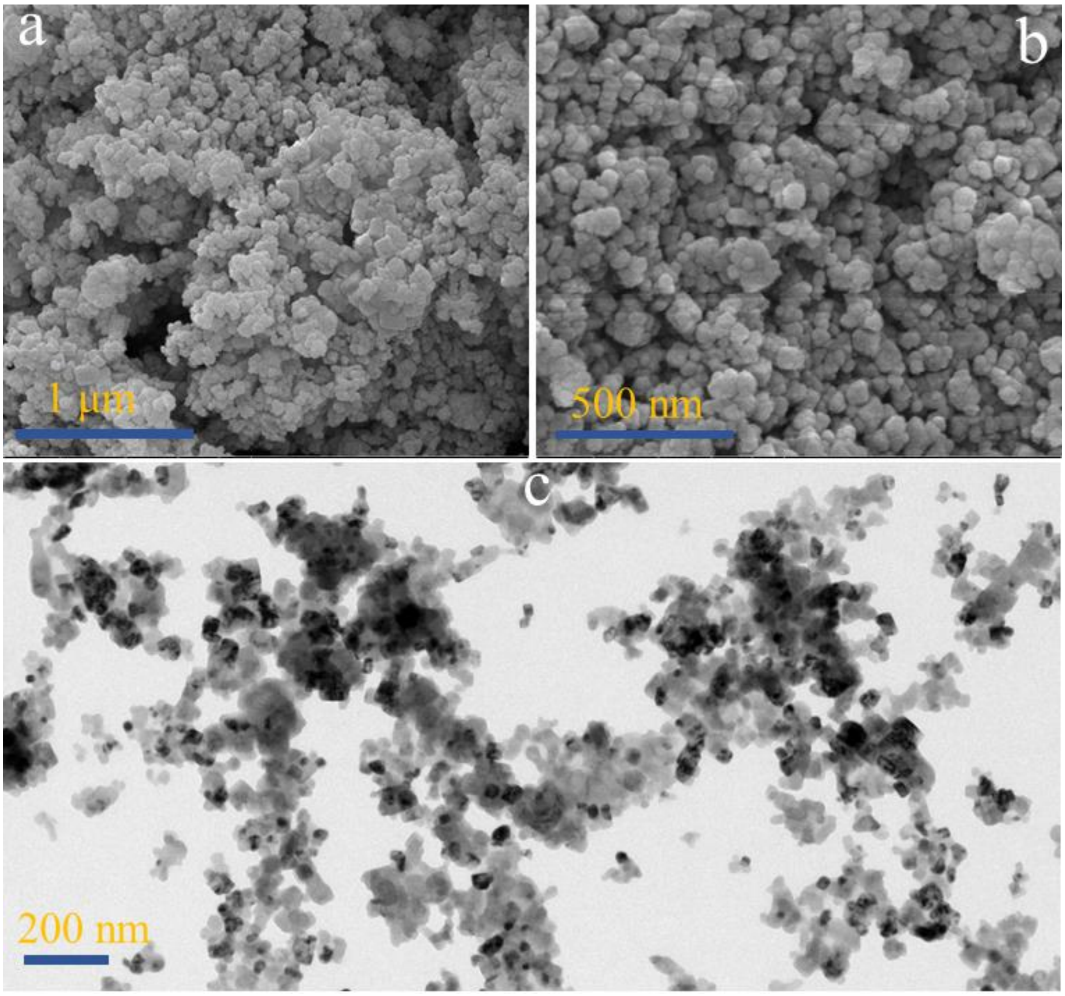

Fig. S3 SEM and TEM images of the $8^{\#}$ sample.

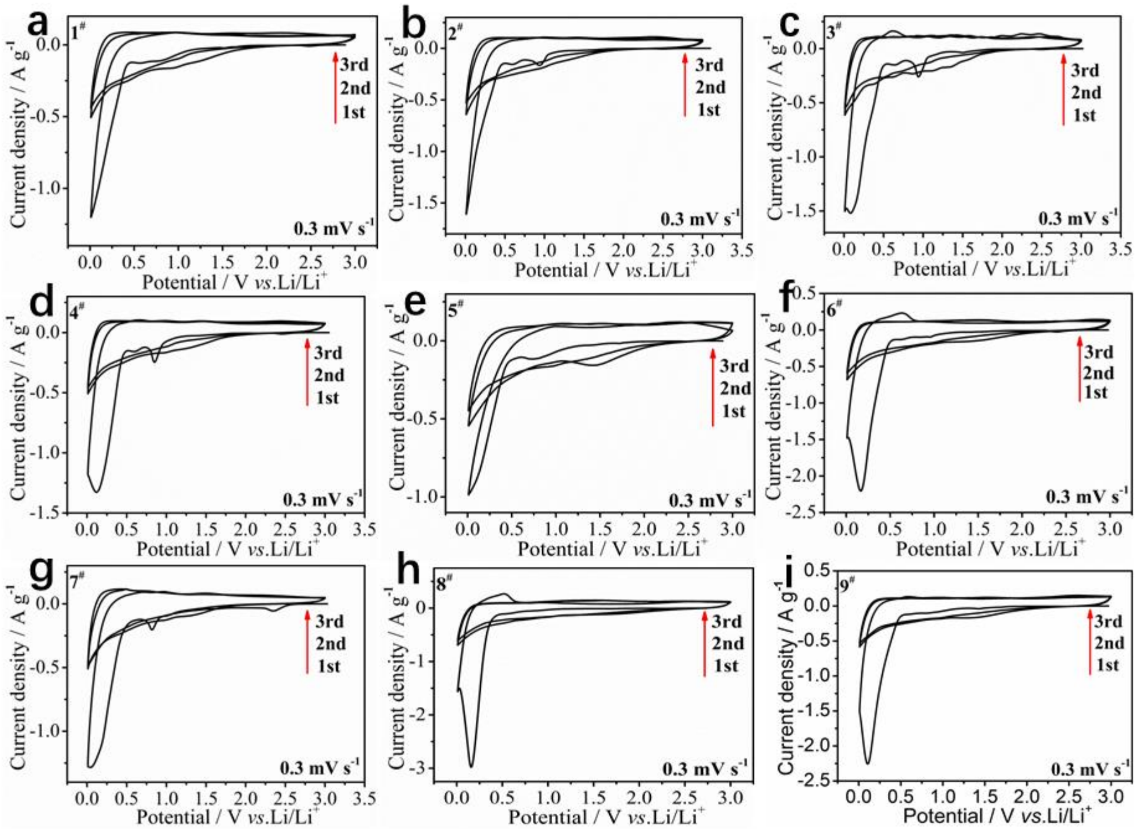

Fig. S4 Performance of Li half-cell: CV plots for the first three cycles of 1#-9# electrodes at 0.3 mV s^{-1} (a-i).

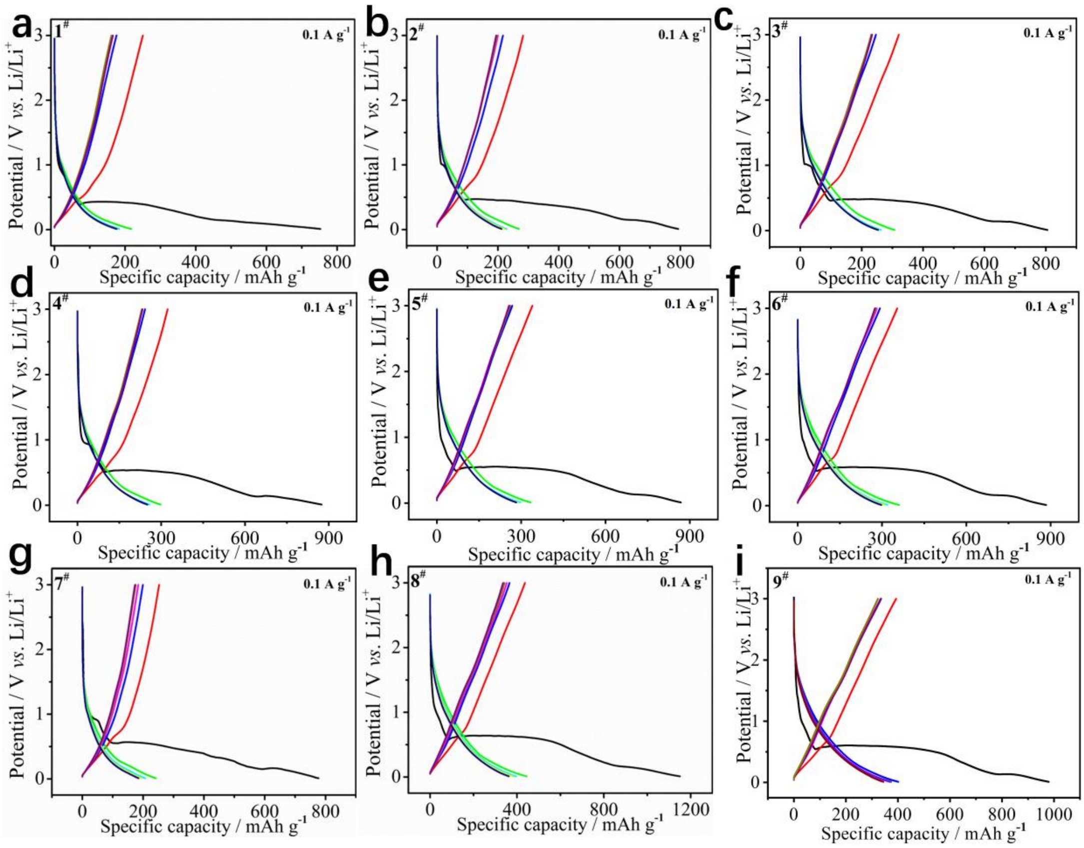

Fig. S5 Performance of Li half-cell: GCD curves for the first five cycles of $1^{\#}$-$9^{\#}$ electrodes at 0.1 A g^{-1} (a-i).

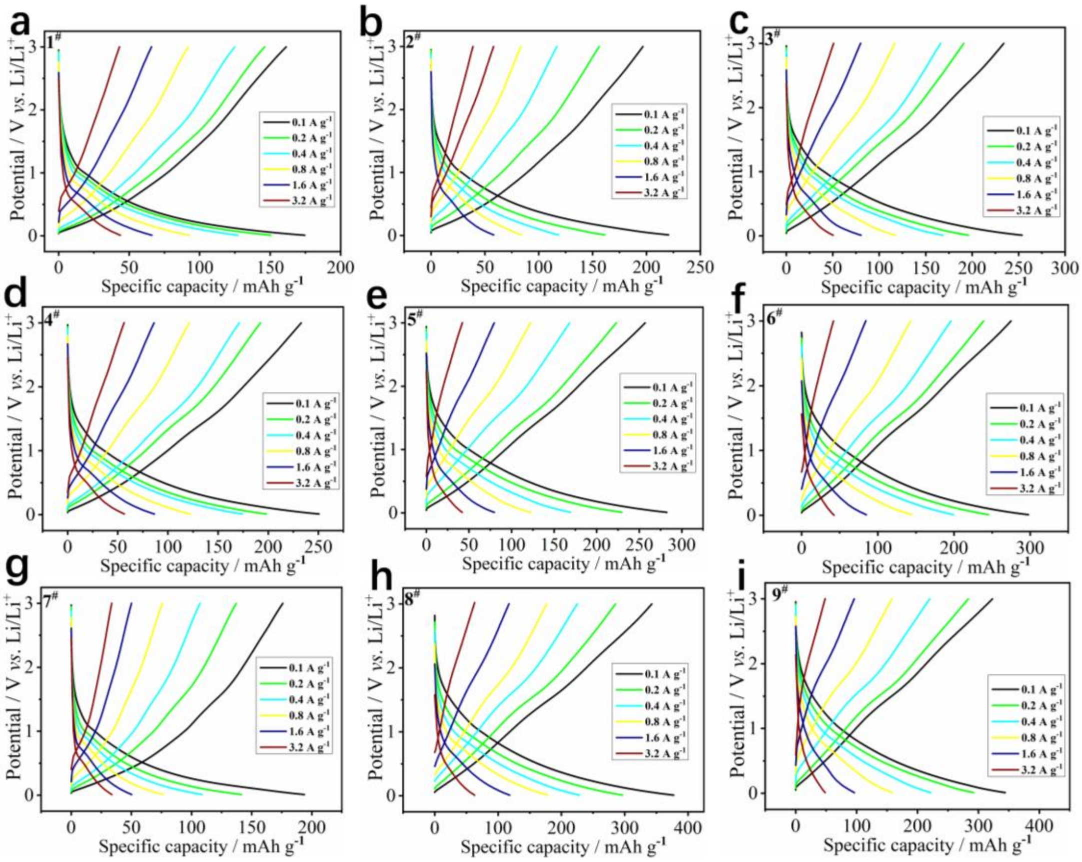

Fig. S6 Performance of Li half-cell: GCD curves for the respective 5[rh] cycles at 0.1~3.2 A g^{-1} of $1^{\#}$-$9^{\#}$ electrodes(a-i).

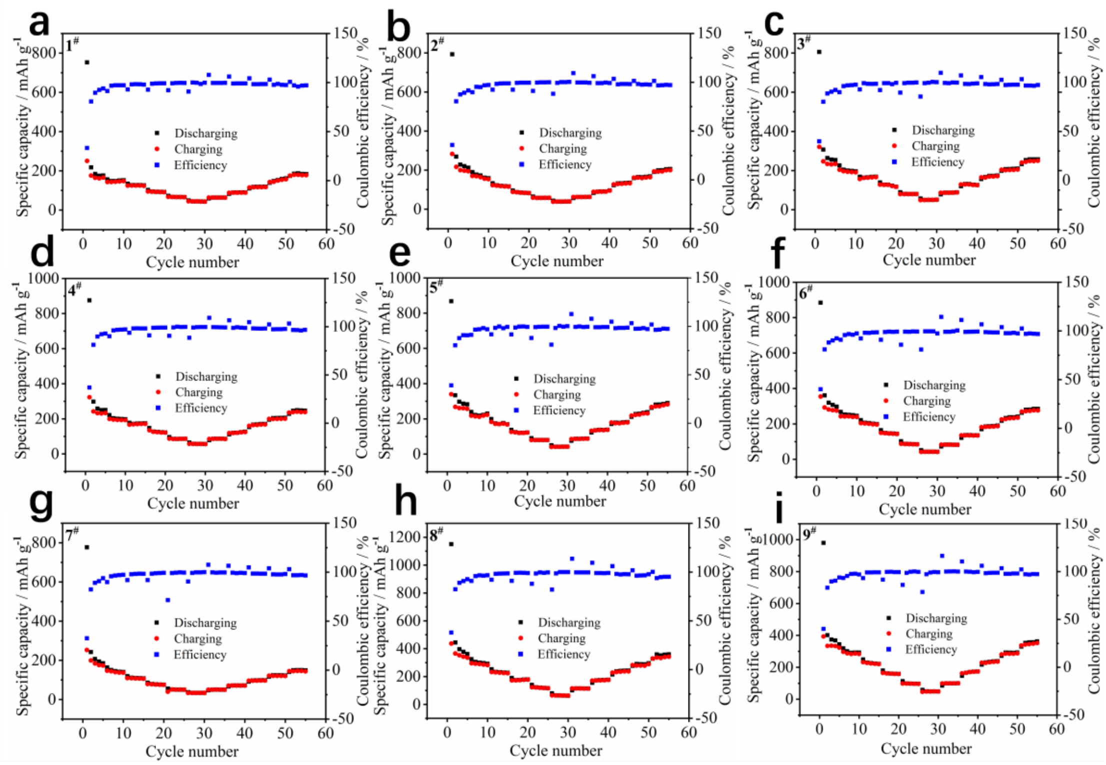

Fig. S7 Performance of Li half-cell: Rate performance and coulombic efficiency of 1#-9# electrodes(a-i).

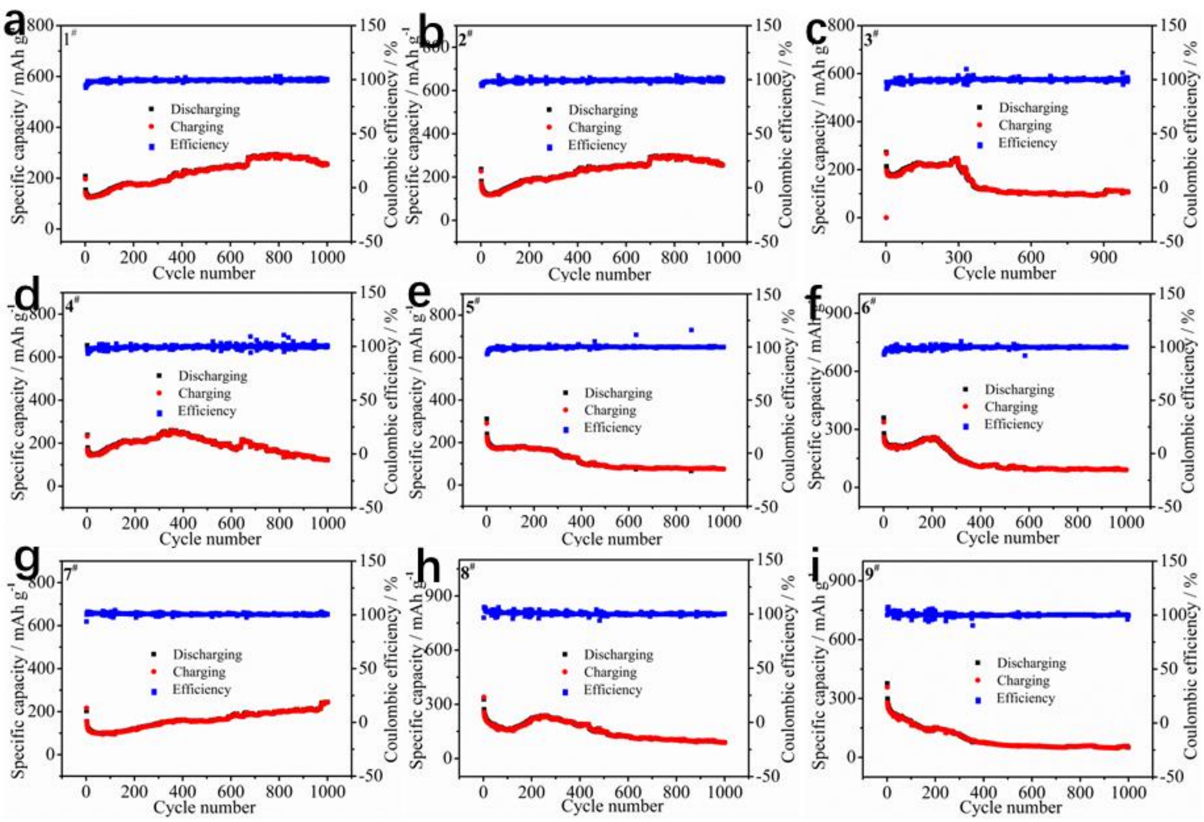

Fig. S8 Performance of Li half-cell: Cycling stability and coulombic efficiency of 1#-9# electrodes at 1 A g^{-1} for 1000 cycles(a-i).

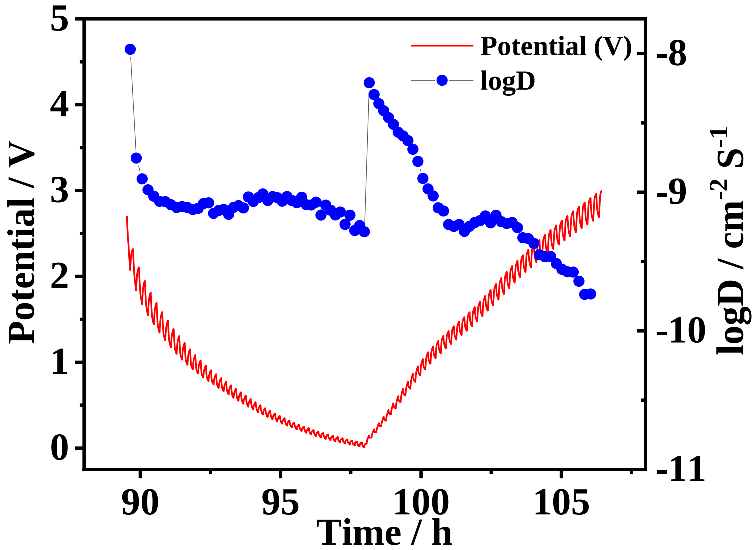

Fig. S9 GITT curves and the corresponding Li^+ diffusion coefficients of $8^{\#}$ electrode (Note: Based on the fifth GITT cycle at 0.1 A g^{-1}, and τ is 300s).

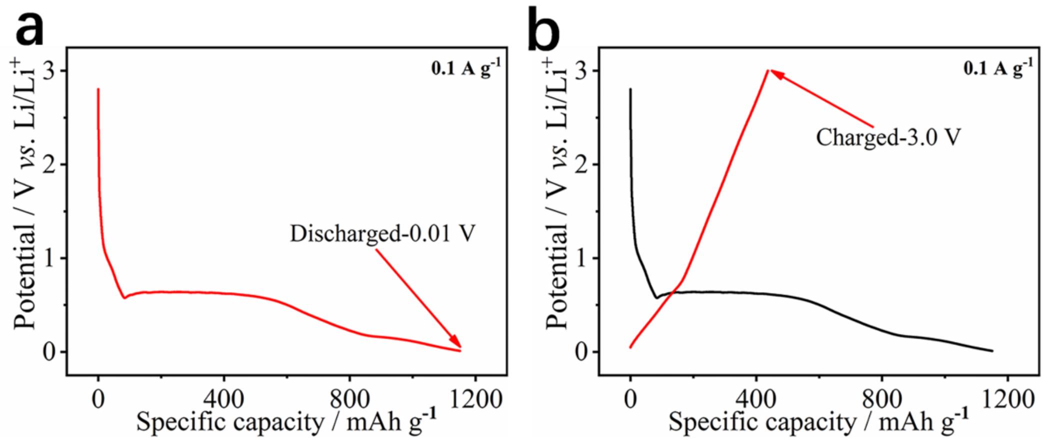

Fig. S10 The 1st segment (a), and 2nd segment (b) GCD curves at 0.1 A g^{-1} of $8^{\#}$ electrode.

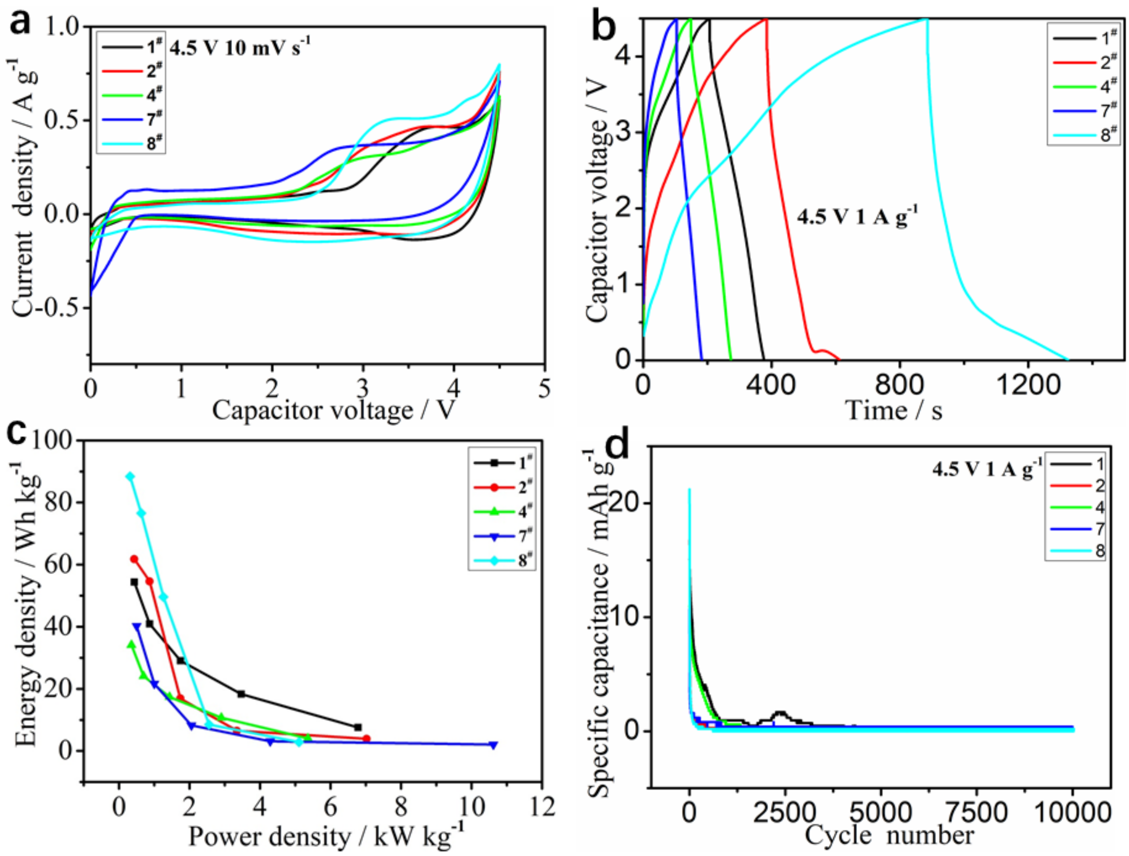

Fig. S11 The CV plots at 10 mV s^{-1} (a), GCD curves at 1 A g^{-1} (b), Ragone plots (c) and cycling behavior for 10000 cycles at 1 A g^{-1} (d) of 1$^{\#}$, 2$^{\#}$, 4$^{\#}$, 7$^{\#}$, 8$^{\#}$//AC LICs

Since the KNCMF-111 (1$^{\#}$, 2$^{\#}$, 4$^{\#}$, 7$^{\#}$ and 8$^{\#}$) electrode materials demonstrate overall superior performance in half-cells, we further constructed LICs using these materials as anode and AC as cathode. Fig. S26 illustrated the electrochemical performance of these LICs under the working voltages of 4.5 V (the GCD curves and m_{+}/m_{-} ratios of the LICs can be seen in the Fig. S27, Table S7). Based on the results, one can see that the 8$^{\#}$//AC LIC exhibits the relatively superior performance among all candidates, but still suffering from an unsatisfactory energy/power densities and very low cycling stability due to lack of precharging (or prelithiated) treatment.

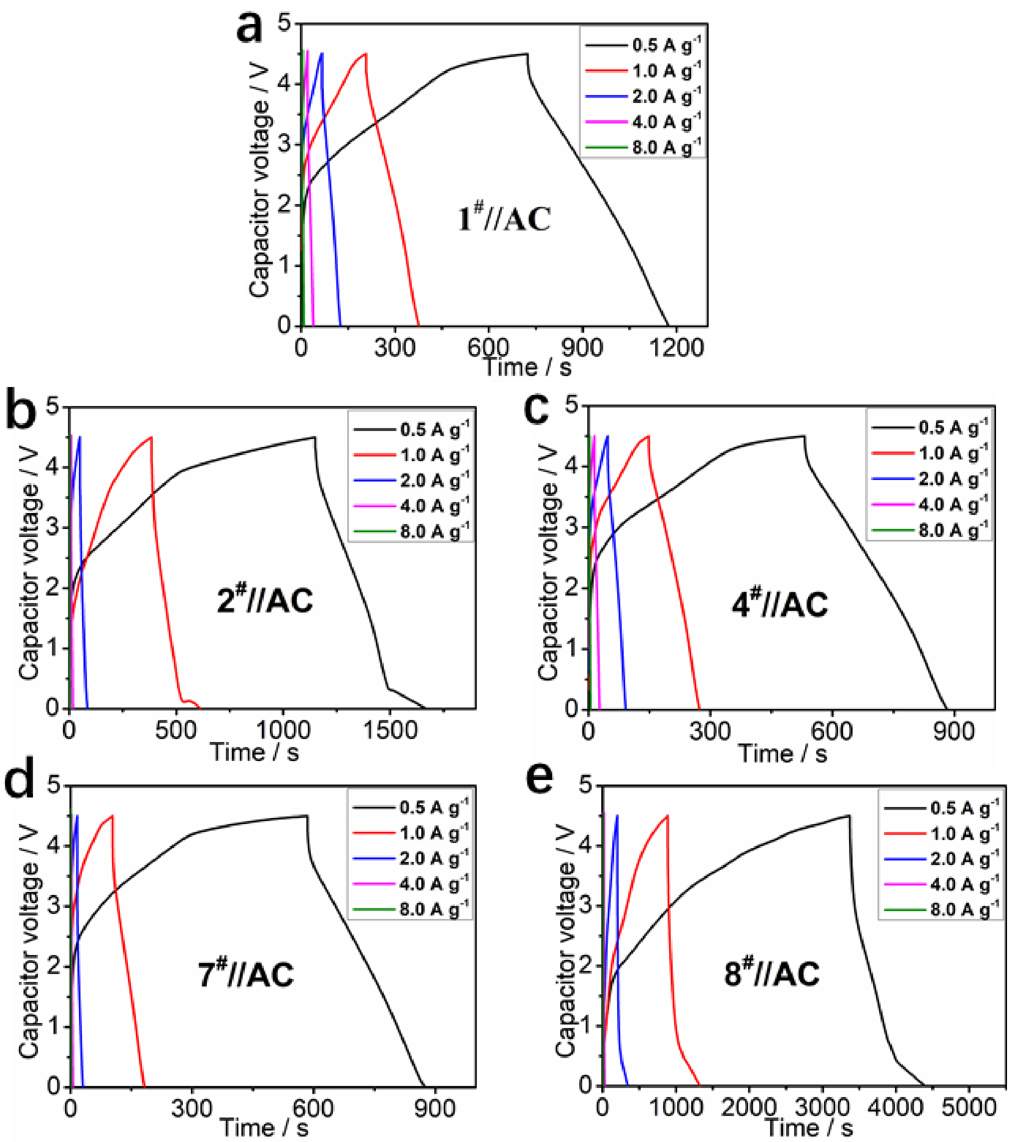

Fig. S12 GCD curves at 0.5-8 A g^{-1} of $1^{\#}$, $2^{\#}$, $4^{\#}$, $7^{\#}$ and $8^{\#}$//AC LICs.

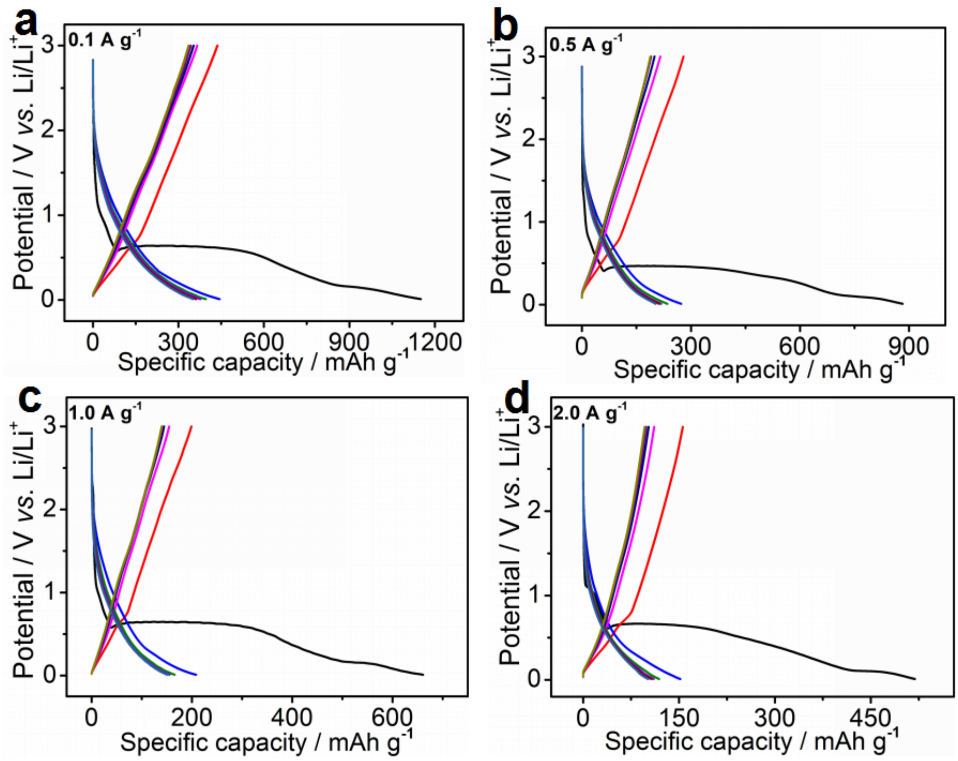

Fig. S13 The typical precharged GCD curves of 8# anode with different precharged current densities

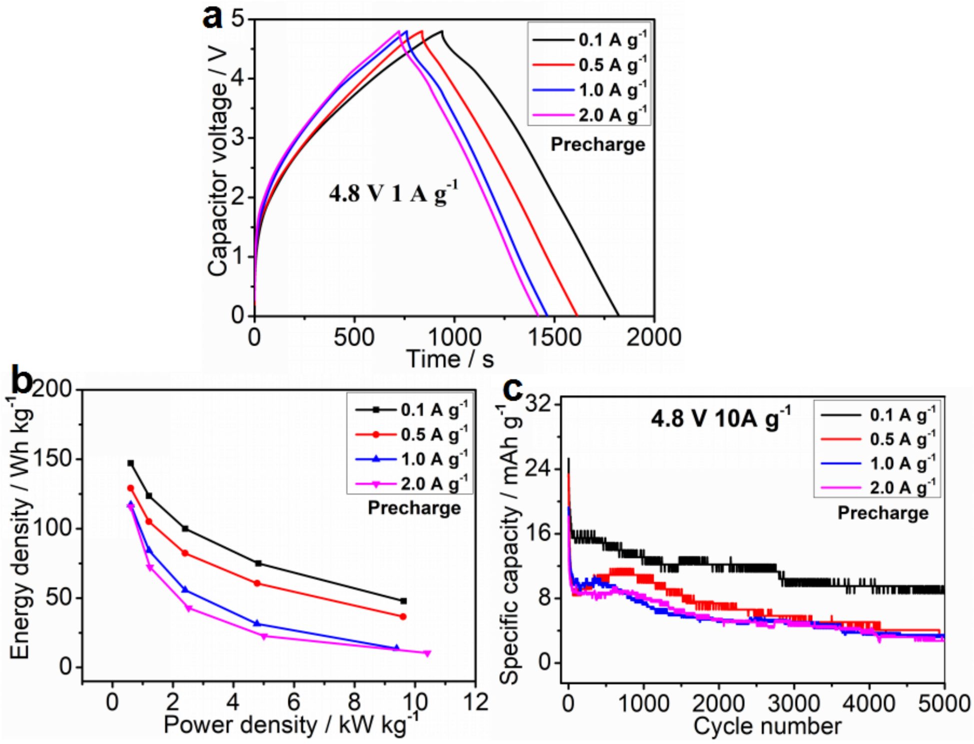

Fig. S14 The GCD curves at 1 A g^{-1} (a), Ragone plots (b), and cycling behavior for 5000 cycles at 5 A g^{-1} in the potential of 0-4.8 V(c) of $8^{\#}$-P//AC LICs with the anode precharged at 0.1-2 A g^{-1}.

In order to optimize the percharging (prelithiation) model, three LICs were fabricated with $8^{\#}$ electrode precharged under 0.1, 0.5, 1 and 2 A g^{-1} in Fig. S28. Based on the performance shown in the Fig. S29, 30, one can see that the precharging current density of 0.1 A g^{-1} is acted as the best precharging model.

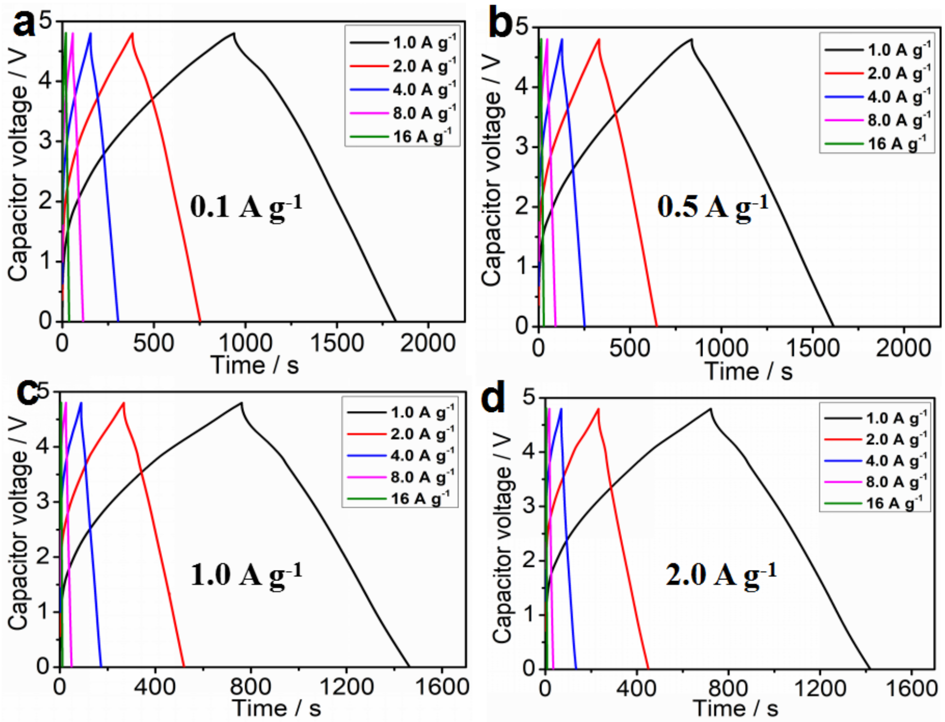

Fig. S15 The GCD curves at 1-16 A g^{-1} of $8^{\#}$-P//AC LICs in the potential of 0-4.8 V with different precharging current densities.

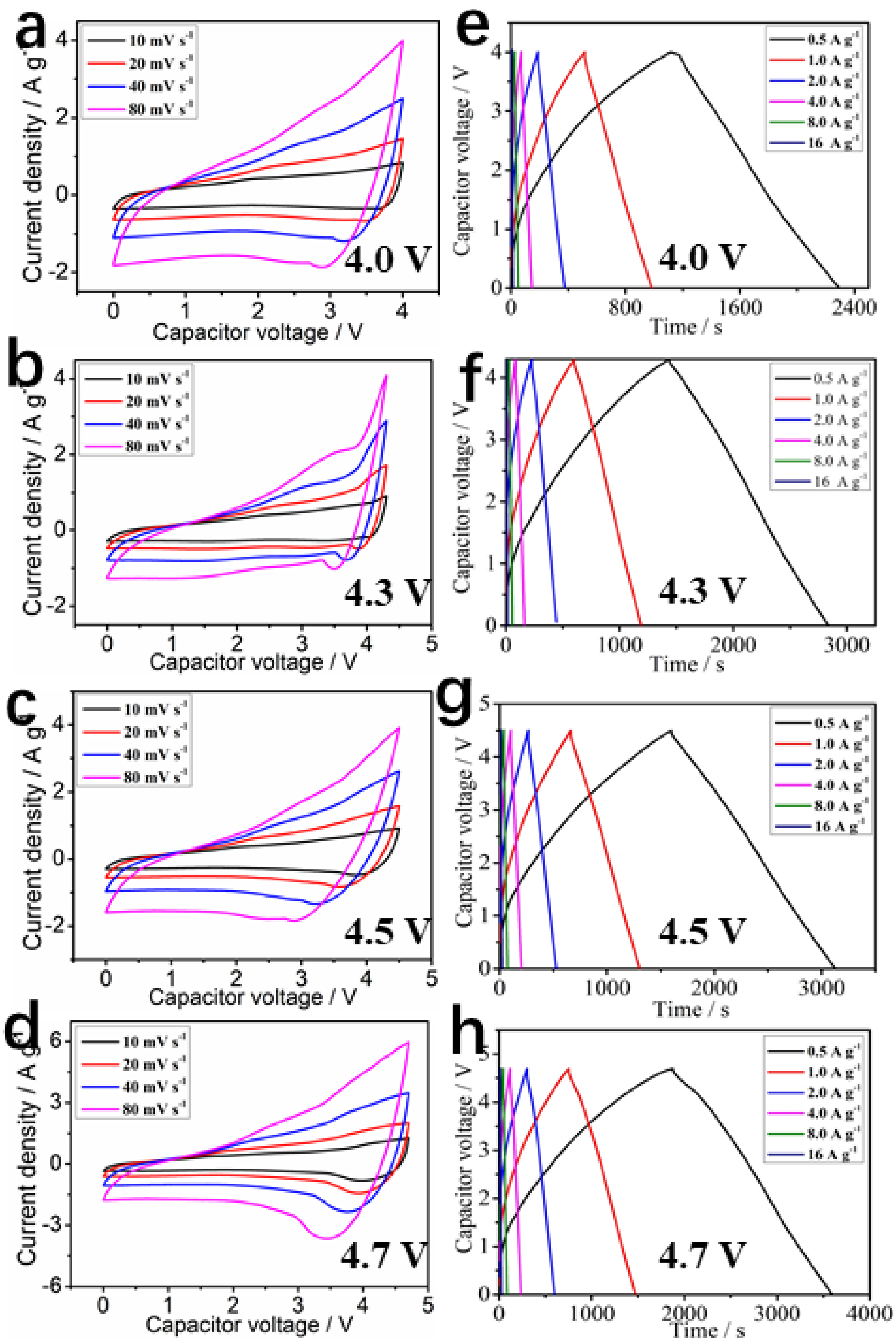

Fig. S16 The CV plots at 10-160 mV s^{-1} and GCD curves at 0.5-16 A $g^{-1}$of $8^{\#}$-P//AC LICs: 4.0 V (a, e), 4.3 V (b, f),4.5 V (c, g) and 4.7 V (d, h).

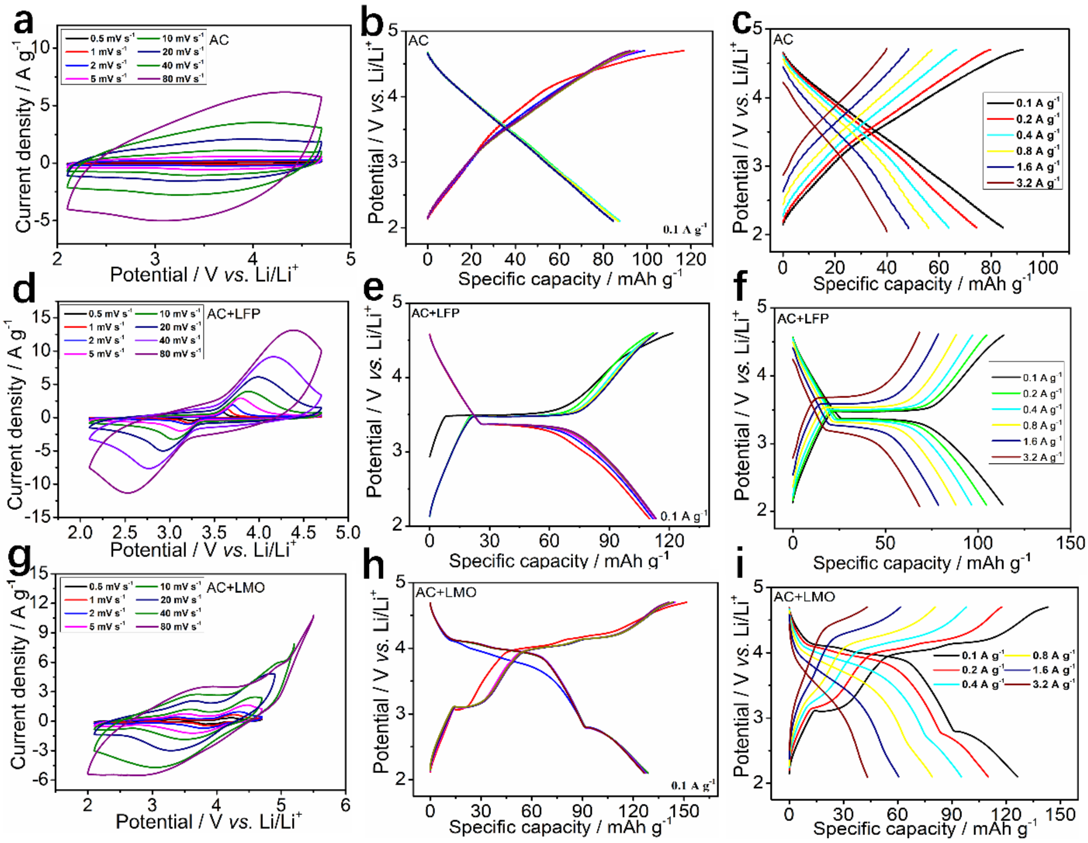

Fig. S17 Performance of AC, AC+LMO and AC+LFP cathode: CV plots at 0.5-80 mV s^{-1} (a, d, g), GCD curves at 1 A g^{-1} (b, e, h) and GCD curves at 0.1-3.2 A g^{-1} (c, f, i).

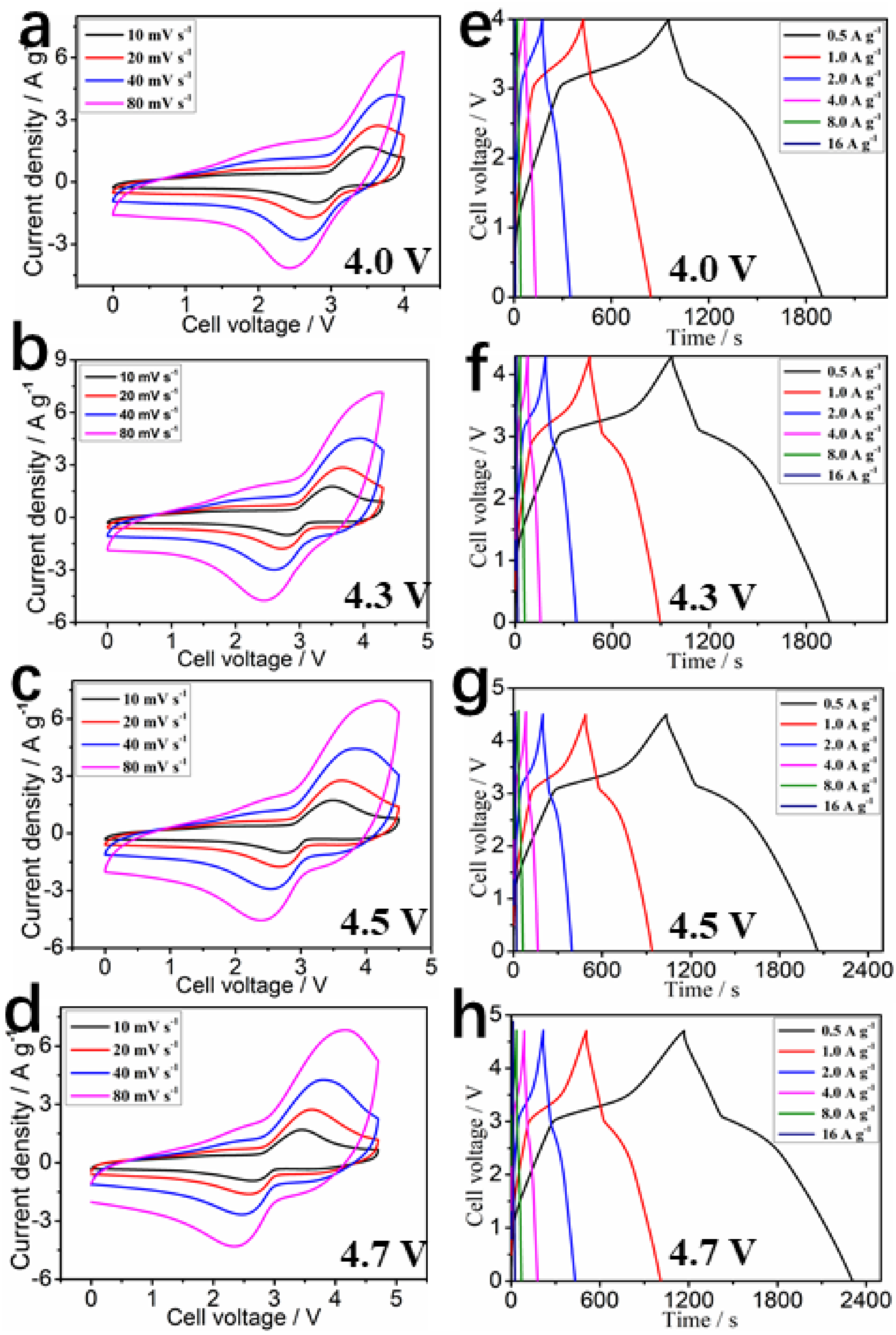

Fig. S18 The CV plots at 10-160 mV s^{-1} and GCD curves at 0.5-16 A $g^{-1}$of $8^{\#}$-P//AC+LFP(1:1) LICBs: 0-4.0 V (a, e), 0-4.3 V (b, f), 0-4.5 V (c, g) and 0-4.7 V (d, h).

Table S1 Chemicals, reagents and materials used in the study.

Chemials, agents and materials	Type	Company	Characteristics
$NiCl_2$•$6H_2O$	AR	SinoPharm	purity≥98.0%
$CoCl_2$•$6H_2O$	AR	SinoPharm	purity≥99.0%
$MnCl_2$•$4H_2O$	AR	SinoPharm	purity≥99.0%
KF•$2H_2O$	AR	SinoPharm	purity≥99.0%
PVP-K30	GR	SinoPharm	/
EG	AR	SinoPharm	purity≥99.0%
NBA	AR	SinoPharm	purity≥99.0%
NPA	AR	SinoPharm	purity≥99.0%
$LiFePO_4$	LFP-NCO	Aleees	D50: 4 ± 2 μm; Tap: 1 ± 0.2 g cm^{-3}; SSA:13 ± 2 m^2 g^{-1}
$LiMn_2O_4$	Battery grade	MTI	D59: 14-22 μm; Tap: 1.8-2.5 g cm^{-3}; ; SSA: 0.5-1.2 m^2 g^{-1}
AC	YEC 8b	FuZhou YiHuan	D50: ~10 μm; Density: >0.4 g cm^{-3}; SSA:2000~2500 m^2 g^{-1}
AB	Battery grade	/	/
NMP	AR	Kermel	purity≥99.0%
PVDF	Battery grade	/	/
Electrolytes	LBC-305-01	CAPCHEM	1 M $LiPF_6$/EC:EMC:DMC (1:1:1) /1% VC
Li plate	15.6*0.45 mm	China Energy	15.6*0.45 mm
Cu foil	200*0.015	GuangZhou JiaYuan	Total thickness: 15 μm; weight: 87 g m^{-2}
Carbon coated-Al foil	222*0.015	GuagZhou NaNuo	Total thickness: 17 μm; Strength: 192 Mpa
Glass microfiber filters	GF/D 2.7 μm; 1823-025	Whatman	Diameter: 25 mm; Thickness: 675 μm; weight: 121 g m^{-2}
Cell components	CR-2032	ShenZhen TianChenHe	/

Table S2 The synthesis conditions of nine KNCMF-111 samples.

Samples	Experimental conditions			
	n(total metal salt)/*n*(KF)	Solvent	Temperature	Time
1#	1:2	EG	160 ℃	6 h
2#	1:2	EG+NBA (1:1)	170 ℃	12 h
3#	1:2	EG+NPA (1:1).	180 ℃	24 h
4#	1:2.5	EG	170 ℃	24 h
5#	1:2.5	EG+NBA (1:1)	180 ℃	6 h
6#	1:2.5	EG+NPA (1:1).	160 ℃	12 h
7#	1:3	EG	180 ℃	12 h
8#	1:3	EG+NBA (1:1)	160 ℃	24 h
9#	1:3	EG+NPA (1:1)	170 ℃	6 h

Note: EG ethylene glycol; NBA n-butyl alcohol; NPA n-propyl alcohol.

Table S3 Specific capacity (mAh g^{-1}) and cycling behavior of $1^{\#}$-$9^{\#}$, AC, AC+LMO (1:1) and AC+LFP (1:1) electrodes in non-aqueous system.

Samples	**Current density/ (A g^{-1})**						**Cycling Retention%/ 1 A g^{-1}/1000 cycles**
	0.1	0.2	0.4	0.8	1.6	3.2	
$1^{\#}$	161.37	146.09	124.93	92.00	65.92	43.18	196
$2^{\#}$	196.71	156.15	116.89	83.48	58.09	39.01	190
$3^{\#}$	233.99	191.08	166.11	116.70	79.92	50.86	58
$4^{\#}$	232.96	192.38	171.26	121.37	86.18	56.62	80
$5^{\#}$	256.82	223.01	168.27	122.20	79.69	42.24	39
$6^{\#}$	274.86	238.94	196.17	143.27	84.36	41.76	39
$7^{\#}$	173.41	136.63	106.00	75.07	49.98	33.68	208
$8^{\#}$	342.81	285.50	225.11	176.89	117.33	63.13	40
$9^{\#}$	323.08	283.38	220.07	157.97	96.26	48.42	20
AC	84.52	74.40	63.69	55.95	48.21	39.88	72
AC+LMO	126.43	110.11	95.28	79.14	60.56	43.27	36
AC+LFP	113.42	104.56	96.56	88.05	78.64	68.43	87

Table S4 The design of electrode mass ratios of LICs and LICBs.

LICs/ LICBs	Q_{m-}(mAh g^{-1})/Q_{m+}(mAh g^{-1}) at 0.1-3.2 A g^{-1}						m_+/m_-
	0.1	0.2	0.4	0.8	1.6	3.2	
1#//AC	1.9	2.0	2.0	1.6	1.4	1.1	**1.7**
2#//AC	2.3	2.1	1.8	1.5	1.2	1.0	**1.7**
4#//AC	2.8	2.6	2.7	2.2	1.8	1.4	**2.3**
7#//AC	2.1	1.8	1.7	1.3	1.0	0.8	**1.5**
8#//AC	4.1	3.8	3.5	3.2	2.4	1.6	**3.1**
8#-P//AC	4.1	3.8	3.5	3.2	2.4	1.6	**3.1**
8#-P//AC+LFP	3.0	2.7	2.3	2.0	1.5	0.9	**1.5***

***Note: The m_+/m_- value was designed considering the excess of anode in the LICBs.**

Table S5 Specific capacity and cycling retention of KNCMF-111($8^{\#}$-P)//AC LICs under different working voltages

Voltages	**Energy density / Wh kg^{-1}**	**Power density / kW kg^{-1}**	**Cycling retention %**
0-4.0 V	79.54-15.18	0.24-7.81	100%/1000/10 A g^{-1} 95%/2000/10 A g^{-1} 90%/3000/10 A g^{-1} 90%/4000/10 A g^{-1}
0-4.3 V	101.60-18.64	0.26-8.39	100%/1000/10 A g^{-1} 95%/2000/10 A g^{-1} 95%/3000/10 A g^{-1} 82%/4000/10 A g^{-1}
0-4.5 V	116.16-25.85	0.27-8.78	92%/1000/10 A g^{-1} 77%/2000/10 A g^{-1} 74%/3000/10 A g^{-1} 70%/4000/10 A g^{-1}
0-4.7 V	136.50-32.10	0.29-9.17	69%/1000/10 A g^{-1} 66%/2000/10 A g^{-1} 60%/3000/10 A g^{-1} 47%/4000/10 A g^{-1}

Table S6 Specific capacity and cycling retention of KNCMF-111(8#-P)//AC+LFP LICBs under different working voltages

Voltages	Energy density / Wh kg^{-1}	Power density / kW kg^{-1}	Cycling retention %
0-4.0 V	153.26-12.09	0.58-10.88	90%/1000/10 A g^{-1} 84%/2000/10 A g^{-1} 84%/3000/10 A g^{-1} 84%/4000/10 A g^{-1}
0-4.3 V	159.25-27.02	0.59-12.16	84%/1000/10 A g^{-1} 84%/2000/10 A g^{-1} 79%/3000/10 A g^{-1} 76%/4000/10 A g^{-1}
0-4.5 V	168.39-41.07	0.59-13.44	83%/1000/10 A g^{-1} 78%/2000/10 A g^{-1} 78%/3000/10 A g^{-1} 70%/4000/10 A g^{-1}
0-4.7 V	184.77-48.53	0.58-13.44	73%/1000/10 A g^{-1} 65%/2000/10 A g^{-1} 60%/3000/10 A g^{-1} 54%/4000/10 A g^{-1}

Table S7 A comparison for the performance of the KNCMF-111 ($8^{\#}$-P)//AC+LFP LICBs in the study with some reported LICs and LIBs.

	System	Working voltage / V	Energy density / Wh kg^{-1}	Power density / kW kg^{-1}	Cycling retention %	Refs.
LICs	3S-Nb_2O_5-HoMSs//AC	1-3.5	93.8-19.6	0.1125-22.5	89%/10000/1 A g^{-1}	[1]
	Soft Carbon//AC/Li_3N	2-4	74.7(Max.)	12.9(Max.)	91%/10000/0.5 A g^{-1}	[2]
	N-NbOC//AC	0-3	86.6-58.7	0.112-3.84	81%/3500/3 A g^{-1}	[3]
	M-Nb_2O_5@C/rGO//AC	0.7-3.2	69.2-4.04	0.248-9.17	94%/2500/0.2 A g^{-1}	[4]
	c$NiCo_2O_4$//VACNFs	1-4.2	136.9	0.2	90%/9000/4 A g^{-1}	[5]
	$Co_3(HHTP)_2$//ACS	0-4	150-64	0.2-10	65%/1000/1 A g^{-1}	[6]
LIBs	Graphite//LiCrTiO4	0.8-2.5	103	/	63%/200/0.25 A g^{-1}	[7]
	Ni/NiO/NC//LiCoO2	2.8-4.2	/	/	90%/100/0.2 C	[8]
	PyPF//$LiFePO_4$	2.5-4	141	/	78%/100/0.05 A g^{-1}	[9]
	m-Si HC/grahite//$LiCoO_2$	2.5-4.2	/	/	73%/100/0.05 C	[10]
	MnO@C-rGO//$LiFePO_4$/Al	0-3.5	/	/	90%/100/0.5 A cm^{-2}	[11]
LICBs	**KNCMF-111($8^{\#}$-P) //AC+LFP**	0-4.0	153.26-12.09	0.58-10.88	84%/3000/10 A g^{-1} 84%/4000/10 A g^{-1}	
		0-4.3	159.25-27.02	0.59-12.16	79%/3000/10 A g^{-1} 76%/4000/10 A g^{-1}	
		0-4.5	168.39-41.07	0.59-13.44	78%/3000/10 A g^{-1} 70%/4000/10 A g^{-1}	
		0-4.7	184.77-48.53	0.58-13.44	60%/3000/10 A g^{-1}	

References

[1] R. Bi, N. Xu, H. Ren, N. Yang, Y. Sun, A. Cao, R. Yu, D. Wang, A Hollow Multi-Shelled Structure for Charge Transport and Active Sites in Lithium-Ion Capacitors, Angew. Chem. Int. Ed. 59 (2020) 4865-4868.

[2] C. Sun, X. Zhang, C. Li, K. Wang, X. Sun, Y. Ma, High-efficiency sacrificial prelithiation of lithium-ion capacitors with superior energy-storage performance, Energy Storage Mater. 24 (2020) 160-166.

[3] S. Hemmati, G. Li, X. Wang, Y. Ding, Y. Pei, A. Yu, Z. Chen, 3D N-doped hybrid architectures assembled from 0D T-Nb_2O_5 embedded in carbon microtubes toward high-rate Li-ion capacitors, Nano Energy 56 (2019) 118-126.

[4] X. Jiao, Q. Hao, X. Xia, Z. Wu, W. Lei, Metal organic framework derived Nb_2O_5@C nanoparticles grown on reduced graphene oxide for high-energy lithium ion capacitors, Chem. Commun. 55 (2019) 2692-2695.

[5] C.-F. Cheng, X. Li, K. Liu, F. Zou, W.-Y. Tung, Y.-F. Huang, X. Xia, C.-L. Wang, B.D. Vogt, Y. Zhu, A high-performance lithium-ion capacitor with carbonized $NiCo_2O_4$ anode and vertically-aligned carbon nanoflakes cathode, Energy Storage Mater. 22 (2019) 265-274.

[6] J. Sun, L. Guo, X. Sun, J. Zhang, Y. Liu, L. Hou, C. Yuan, Conductive Co-based metal–organic framework nanowires: a competitive high-rate anode towards advanced Li-ion capacitors, J. Mater. Chem. A 7 (2019) 24788-24791.

[7] K. Subramanyan, S. Natarajan, Y.-S. Lee, V. Aravindan, Exploring the usage of $LiCrTiO_4$ as cathode towards constructing 1.4 V class Li-ion cells with graphite anode recovered from spent Li-Ion battery, Chem. Eng. J. 397 (2020) 125472.

[8] S. Archana, M. Athika, P. Elumalai, Supercapattery and full-cell lithium-ion battery performances of a [Ni(Schiff base)]-derived Ni/NiO/nitrogen-doped carbon heterostructure, New J. Chem. 44 (2020) 12452-12464.

[9] S. Mamidi, A. Gangadharan, C.S. Sharma, Graphite coated pyrolyzed filter paper as a low-cost binder-free and freestanding anode for practical lithium-ion battery application, Electrochim. Acta 310 (2019) 222-229.

[10] T. Yoon, T. Bok, C. Kim, Y. Na, S. Park, K.S. Kim, Mesoporous Silicon Hollow Nanocubes Derived from Metal–Organic Framework Template for Advanced Lithium-Ion Battery Anode, ACS Nano 11 (2017) 4808-4815.

[11] G. Zhong, J. Yu, P. Zhuang, M. Jin, Y. Fu, X. Ma, Ultralong MnO@C nanowires with internal voids anchored between graphene as a robust high performance anode for flexible Li-Ion battery, Electrochim. Acta 296 (2019) 276-282.